Draft version May 28, 2025
Typeset using LaTeX **default** style in AASTeX7

A candidate for True Type-2 AGN without hidden central BLRs Identified by central Tidal Disruption Event

Ying Gu [1], Qi Zheng [2], Pei-zheng Cheng [1], Xiao Li [1], Xing-Qian Cheng [1], Xue-Guang Zhang* [1] and En-Wei Liang* [1]

[1] *Guangxi Key Laboratory for Relativistic Astrophysics, School of Physical Science and Technology, Guangxi University, Nanning 530004, People's Republic of China*
[2] *School of Physics and technology, Nanjing Normal University, No. 1, Wenyuan Road, Nanjing, 210023, People's Republic of China*

ABSTRACT

In this manuscript, through applications of TDE (tidal disruption event) expected variability properties, a potential candidate for True type-2 AGN without hidden central broad line regions (=TT2AGN) is reported in the SDSS J233454.07+145712.9 (=SDSS J2334). Through analyzing the 20-years optical light curves of SDSS J2334 from different Sky Survey projects, a TDE is preferred with a $4.7M_{\odot}$ main-sequence star tidally disrupted by the central BH with mass $11.7 \times 10^6 M_{\odot}$, indicating that central region within distance about 20 light-days to central BH in SDSS J2334 is directly in the line-of-sight. Moreover, AGN activities in SDSS J2334 can be confirmed through applications of BPT diagrams. Meanwhile, comparing virial BH mass determined through assumed broad Balmer emission components and M-sigma expected BH mass by well measured stellar velocity dispersion through stellar absorption features, optical broad emission lines in SDSS J2334 are disfavored with confidence level higher than 6σ. Therefore, combining the unique properties of the TDE and the spectroscopic results with only narrow emission lines, SDSS J2334 can be well identified as a potential candidate for a TT2AGN. The results indicate the to detect TDE expected flares in normal Type-2 AGN classified by spectroscopic results should be a new practicable method for identifying TT2AGN.

Keywords: Galaxies (573) — Active galactic nuclei (16) — Tidal disruption (1696) — Quasars (1319)— Time domain astronomy (2109)

1. INTRODUCTION

Active galactic nuclei (AGNs) are broadly classified into two different types within the Unified Model (UM), i.e., Type 1 AGNs have broad line regions (BLRs) and narrow-line regions (NLRs) in the line of sight, while Type 2 AGNs are obscured by a dusty torus, with only the NLRs observed (R. Antonucci 1993; C. M. Urry & P. Padovani 1995). Although the UM successfully explains broad observations, some additional ingredients are needed in order to take into account all the observational evidence (e.g. S. Veilleux et al. (1997); H. D. Tran (2001); N. L. Zakamska et al. (2005); B. C. Wilhite et al. (2005); C. W. Yip et al. (2009); D. Savić et al. (2018)). More recent detailed discussions on the UM can be found in H. Netzer (2015). Even after considering necessary modifications, the UM is an incomplete picture for accommodating the data (e.g., S. Gezari et al. (2006); M. Elitzur (2012)). As proposed by H. D. Tran (2001, 2003), a significant fraction of Type 2 AGN does not show hidden BLRs, even when high-quality spectropolarimetric data are available, leading to the called True Type-2 AGN (TT2AGN) in the manuscript. Here, TT2AGN, also called Type-2 AGN with non-hidden BLRs or AGN without BLRs or unobscured Type-2 AGN or naked AGN in the literature, means the AGN which has no central BLRs, not the AGN with heavily obscured central BLRs leading to the classified Type 1.9 AGN. Since then, unobscured narrow-line AGN were well studied for identifying TT2AGN without hidden central BLRs as predicted by the UM from both the observations (M. R. S. Hawkins 2004; M. Brightman & K. Nandra 2008;

Corresponding author: Xue-Guang Zhang; En-Wei Liang
xgzhang@gxu.edu.cn; lew@gxu.edu.cn

X.-X. Huang et al. 2011; S. Bianchi et al. 2012; L. C. Ho et al. 2012; M. Valencia-S. et al. 2012; X.-G. Zhang 2014; A. J. Barth et al. 2014; K. Ichikawa et al. 2015; E. Pons & M. G. Watson 2016; X. Zhang et al. 2021) and theoretical analysis (M. Elitzur & L. C. Ho 2009; X. Cao 2010; K. Ichikawa et al. 2015; Y. Li et al. 2015; M. Elitzur & H. Netzer 2016). However, the existence of TT2AGN is still under debating (T. Nagao et al. 2004; R. Antonucci 2012; K. Ichikawa et al. 2015). For example, observations with HST suggest that the previously accepted TT2AGN candidate, NGC 3147, is definitely not a TT2AGN (S. Bianchi et al. 2019). Therefore, identifying candidates of TT2AGN remains extremely challenging.

Based on the UM expected obscurations on central AGN activity in normal type-2 AGN, there should be no photometric variability in normal Type-2 AGN. Therefore, an effective approach to identify a TT2AGN candidate is to directly search for significant flux variability of normal Type-2 AGN (M. R. S. Hawkins 2004; A. J. Barth et al. 2014). Here, Tidal disruption events (TDEs) can produce a bright flare that may last for months to years (e.g., M. J. Rees 1988; A. Merloni et al. 2015; B. Trakhtenbrot et al. 2019; X.-G. Zhang 2022). These flares occur when a star's orbit passes within the tidal radius of a supermassive black hole (SMBH), leading TDEs as reliable indicators of BH accreting systems located within dozens to hundreds of Schwarzschild radii from central SMBHs (M. J. Rees 1988; D. N. Burrows et al. 2011; S. Gezari et al. 2012; S. van Velzen et al. 2016; S. Mattila et al. 2018; S. Gezari 2021). For example, the well-known TDE ASASSN-14li has bright flares, lasting for six months (J. S. Brown et al. 2017), and has been extensively studied in recent years(T. Wevers et al. 2024; X. Zhang 2024). Several samples of TDE candidates have been identified (S. van Velzen et al. 2021; S. Sazonov et al. 2021; E. Hammerstein et al. 2023; Y. Yao et al. 2023). A TDE observed in a normal Type 2 AGN classified by spectroscopic properties should be a smoking-gun of a TT2AGN.

In this manuscript, considering the unusual outburst events in SDSS J233454.07+145712.9 (hereafter SDSS J2334) which has been reported in A. J. Drake et al. (2019), combining with spectroscopic emission line properties. We report the discovery of a TDE candidate in the type-2 AGN SDSS J2334, providing interesting clues to support SDSS J2334 as a potential candidate for TT2AGN. The manuscript is organized as follows. Section 2 presents the TDE candidate discovered from the optical long-term photometric light curves of SDSS J2334. Section 3 presents our spectroscopic analysis for SDSS J2334. Conclusions are presented in Section 4. The cosmological parameters of H_0=70 km s^{-1} Mpc^{-1}, Ω_m=0.3, and Ω_Λ=0.7 are adopted.

2. A TDE CANDIDATE IN THE LONG-TERM LIGHT CURVES OF SDSS J2334

SDSS J2334 at redshift $z = 0.1075$ has its 18years-long light curves shown in Fig. 1, including the Catalina Sky Survey (CSS) (A. J. Drake et al. 2009) V band light curve with MJD from 53554 (Jul. 2005) to 56587 (Oct. 2013), the Palomar Transient Factory (PTF) (N. M. Law et al. 2009) R band light curve with MJD from 55023 (Jul. 2009) to 55499 (Oct. 2010), the PanSTARRS (Panoramic Survey Telescope & Rapid Response System) $grizy$ band light curves with MJD from 55092 (Sep. 2009) to 56651 (Dec. 2013). and the Zwicky Transient Facility (ZTF E. C. Bellm et al. (2019)) r band light curve with MJD from 58268 (May 2018) to 60245 (Oct. 2023)[3] Through the shown light curves, two interesting points can be well confirmed. First, there is an outburst event with MJD-53000 from about 2100 (Oct. 2009) to about 3500 (Sep. 2013), not only similar as previously reported results in A. J. Drake et al. (2019) through the CRTS (Catalina Real-Time Survey) V-band light curve, but also re-confirmed by the PanSTARRS and PTF light curves. Second, except the outburst event, SDSS J2334 is at quiescent state with none apparent variabilities, not only confirmed by the CSS V-band light curve with MJD-53000 smaller than 2000, but also confirmed by the more recent ZTF r-band light curves. This is further supported by ZTF g-band forced photometry (MJD 58290-60694) (F. J. Masci et al. 2023), which shows no post-outburst variability (Appendix Fig A).

For the outburst event with MJD-53000 from 2100 to 3500, there is a steep rise and then followed by a smoothly declined trend, similar as optical TDEs expected variability patterns. To reveal the nature of the outburst, we further describe the light curves with the conventional theoretical TDE model. We adopt the public codes of TDEFIT and MOSFIT (J. Guillochon et al. 2014, 2018; B. Mockler et al. 2019) on theoretical TDE model. Similar as what we have recently done in Y. Gu et al. (2024); X.-G. Zhang (2024); X. Zhang (2025) considering theoretical TDE model expected time dependent templates of viscous delayed accretion rates applied in simple black-body photosphere model, we outline the following procedure to describe the optical outburst event by theoretical TDE model.

[3] The ZTF-g/i band light curves were not collected, as their variability is similar to that of the ZTF-r band.

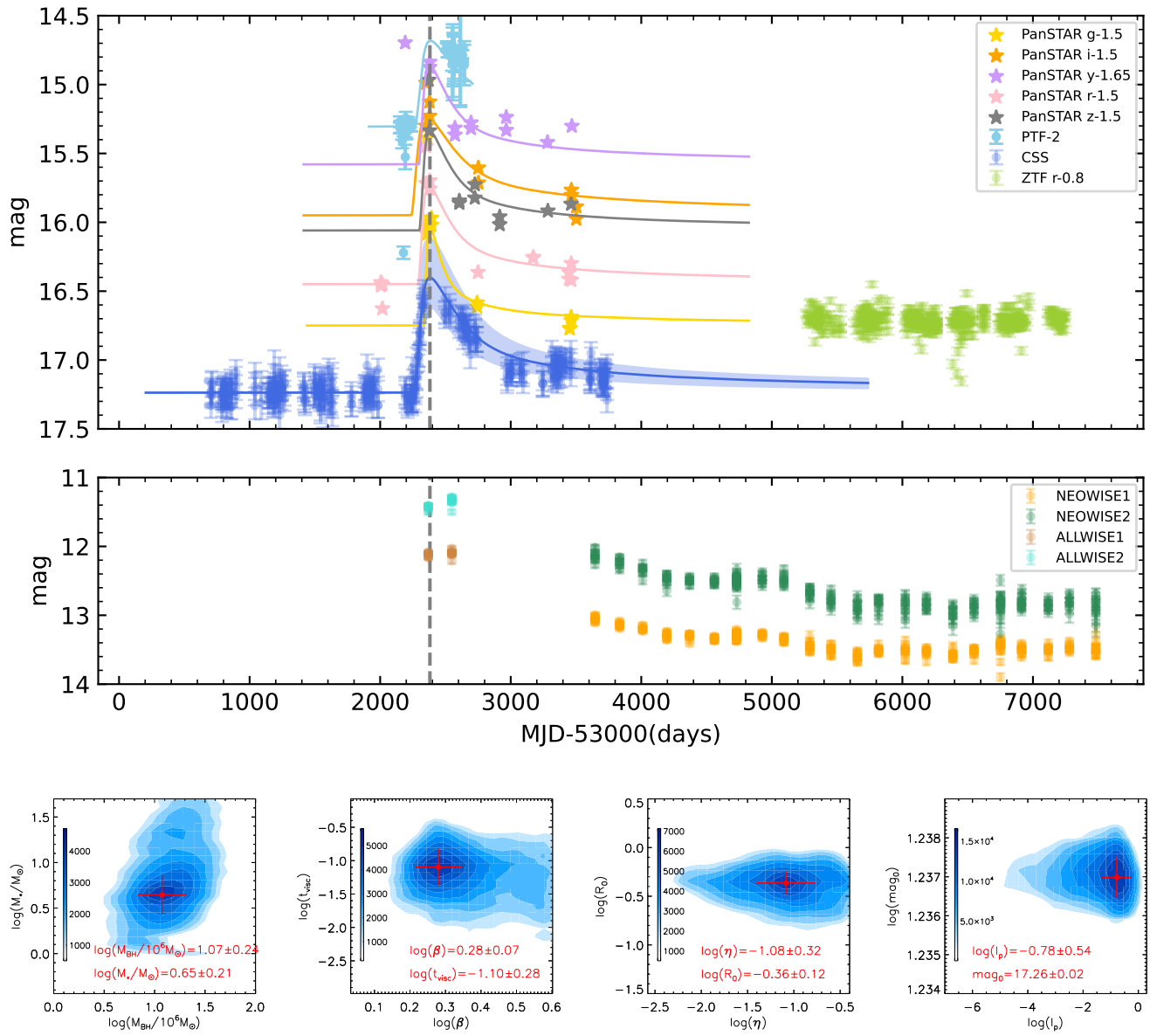

Figure 1. The top panel shows the CSS V-band light curve (blue symbols) and the TDE model determined best descriptions (solid blue line) and the corresponding confidence bands (blue shaded area) determined by uncertainties of the model parameters. The remaining light curves are collected from the other projects, as shown in the legend in the top right corner. Solid lines in different colors show the best descriptions to the light curves after accepting the TDE model parameters applied to describe the CSS V band light curve, except for the ZTF r-band light curve. The middle panel displays the WISE infrared light curves of SDSS J2334 in the W1 and W2 bands, with different colors representing different observational data (see top-right legend). In the top two panels, the grey dashed line shows the peak positions preferred by the standard TDE model. Bottom panels show the MCMC determined two-dimensional distributions of TDE model parameters. In each bottom panel, solid circle plus error bars in red mark the accepted values and the corresponding uncertainties of the model parameters which are marked in red characters in bottom region.

First, the viscous-delayed accretion rates $\dot{M}_a$ are created based on the dM/dE (the fundamental elements in the public code of TDEFIT/MOSFIT) and the viscous delay effects (J. Guillochon & E. Ramirez-Ruiz 2013; B. Mockler et al. 2019). A standard TDE event, in which a main-sequence star with $M_* = 1\mathrm{M}_\odot$ is tidally disrupted by a BH with $M_{BH} = 10^6\mathrm{M}_\odot$, is considered. We construct the standard templates of the time-dependent viscous-delayed accretion rate $\dot{M}_a(T_v, \beta)$, where β is the impact parameter and T_v is the viscous time.

Second, for common TDEs, the actual accretion rate at time t can be estimated using scaling relations, which depend on the black hole mass and the stellar parameters (B. Mockler et al. 2019):

$$\begin{aligned} \dot{M} &= M_{\rm BH,6}^{-0.5} \times M_*^2 \times R_*^{-1.5} \times \dot{M}_a(T_v, \beta) \\ t &= (1+z) \times M_{\rm BH,6}^{0.5} \times M_*^{-1} \times R_*^{1.5} \times t_a(T_v, \beta), \end{aligned} \tag{1}$$

where central BH mass $M_{\rm BH,6}$ is in units of $10^6 {\rm M}_\odot$, stellar mass M_* is in units of ${\rm M}_\odot$, stellar radius R_* is in units of ${\rm R}_\odot$, z represents redshift of the host galaxy of the TDE. Additionally, we adopt the known mass-radius relation for main-sequence stars from C. A. Tout et al. (1996).

Third, based on the standard blackbody photosphere (e.g., B. Mockler et al. 2019), the time-dependent emission spectrum in the rest frame can be calculated as

$$\begin{aligned} T_p(t) &= \left(\frac{L}{4\pi\sigma_{SB}R_p^2}\right)^{1/4} = \left[\frac{\eta\dot{M}(t)c^2}{4\pi\sigma_{SB}R_p^2}\right]^{1/4}, \\ R_p(t) &= R_0 \times a_p (L/L_{\rm Edd})^{l_p} = R_0 \times a_p \left[\frac{\eta\dot{M}(t)c^2}{1.3\times10^{38}M_{\rm BH}}\right]^{l_p}, \\ a_p &= \left[GM_{\rm BH} \times (\frac{t_p}{2\pi})^2\right]^{1/3}, \\ F_\lambda(t) &= \frac{2\pi hc^2}{\lambda^5}\frac{1}{e^{hc/(k\lambda T_p(t))}-1}\left[\frac{R_p(t)}{D(z)}\right]^2, \end{aligned} \tag{2}$$

where $T_p(t)$ and $R_p(t)$ are the time-dependent effective temperature and radius of the photosphere, respectively. $R_p(t)$ ranges from the minimum $R_{\rm isco}$ (event horizon radius) to a_p (maximum semimajor axis) of the accreting mass. L is the time-dependent bolometric luminosity given by $L = \eta\dot{M}(t)c^2$, $L_{\rm Edd}$ represents the Eddington luminosity, η represents the energy transfer efficiency that is less than 0.4 (J. Guillochon et al. 2014; B. Mockler et al. 2019), $\sigma_{\rm SB}$ is the Stefan-Boltzmann constant, l_p represents the power-law exponent and t_p is the time information of the peak accretion. $D(z)$ is the luminosity distance at redshift z. Then, time-dependent apparent CSS-V band magnitudes can be well determined through the $F_\lambda(t)$ in the observer frame convolving with the accepted transmission curves of the CSS-V band filter.

The free parameters of the TDE model include $M_{\rm BH}$, M_* (the corresponding stellar radius R_* calculated by the mass-radius relation), β, T_v, η, R_0, l_p, and the magnitude of the host galaxy in the CSS-V band (mag_0). Then, through the known Maximum likelihood method combined with the Markov Chain Monte Carlo (MCMC) technique (D. Foreman-Mackey et al. 2013), the best descriptions to the CSS V band light curve of SDSS J2334 can be determined and shown in the top panel of Fig. 1. Meanwhile, the MCMC technique determined posterior distributions of the model parameters are shown in the bottom panel of Fig. 1, leading the determined model parameters with a polytropic index of $\gamma = 4/3$ to be: $\log(M_{\rm BH,\,6}) \sim 1.07 \pm 0.24$, $\log(M_*/M_\odot) \sim 0.65 \pm 0.21$, $\log(\beta) \sim 0.28 \pm 0.07$, $\log(T_v) \sim -1.10 \pm 0.28$, $\log(\eta) \sim -1.08 \pm 0.32$, $\log(R_0) \sim -0.36 \pm 0.12$, $\log(l_p) \sim -0.78 \pm 0.54$ and $mag_0 \sim 17.26 \pm 0.02$. Furthermore, by applying the obtained fitting parameters to the light curves in the PTF-R and PanSTARRS-$grizy$ bands (the host galaxy magnitude in each band is treated as a free parameter), reasonable fitting results are also obtained, as shown in the middle panel of Fig 1.

Based on the theoretical TDE model determined results, the expected tidal disruption radius is about $7R_G$ (Schwarzschild radius). Once the central TDE can be expected, spatial size of the geometric structure of TDE debris can be simply checked. The TDE debris in SDSS J2334 around MJD-53000=3000 5000 have outer distance (J. Guillochon et al. 2014)

$$R_{out} \sim 2 \times (\frac{GM_{BH}t^2}{\pi^2})^{1/3} \sim 7.6 - 16.6{\rm light-days} \tag{3}$$

with G as gravitational constant and M_{BH} as the BH mass in units of ${\rm M}_\odot$, clearly indicating the central region around the central BH of SDSS J2334 is in the direction of our sight.

To conclude this section, we note that it seems that a 'bump' flare has been observed about ~ 900 days after the peak. Such rebrightening bump phenomena in optical band have been observed in some TDEs and candidates such as SDSS

J0159+0033 (A. Merloni et al. 2015), IRAS F01004-2237 (L. Sun et al. 2024), and some recent TDEs reported in Y. Yao et al. (2023). Several physical mechanisms have been proposed to explain the rebrightening bumps in TDEs, such as the transition from super-Eddington to sub-Eddington accretion (L. E. Strubbe & E. Quataert 2009) and delayed disk formation (X.-L. Liu et al. 2022). Recently, H. Guo et al. (2025) have collected a small sample of TDEs exhibiting prominent rebrightening bumps and have found that the model combining stream collisions and delayed accretion disk formation could provide a unified explanation for diverse TDE observations. We should note that the 'bump' in SDSS J2334 falls within the confidence interval, but its character is less prominent compared to the aforementioned TDEs. Therefore, we only consider theoretical models of TDEs in our analysis. As these discussions are beyond the scope of this manuscript, we will not explore them further.

3. SPECTROSCOPIC RESULTS OF SDSS J2334

SDSS J2334 has its SDSS spectrum (median signal-to-noise about 18, plate-mjd-fiberid=0747-52234-0400) observed in MJD=52234 (Nov. 2001, far away from the duration of the expected central TDE) collected from the Sloan Digital Sky Survey (SDSS) DR16 (R. Ahumada et al. 2020) and shown in top panel of Fig. 2, with apparent stellar absorption features. In order to measure emission lines, the well accepted SSP (Simple Stellar Populations) method (G. Bruzual A. & S. Charlot 1993; G. Bruzual & S. Charlot 2003; R. Cid Fernandes et al. 2005; M. Cappellari 2017) is applied to determine host galaxy contributions and intrinsic AGN continuum emissions, considering the 39 simple stellar population templates (G. Kauffmann et al. 2003; G. Bruzual & S. Charlot 2003) for host galaxy contributions plus a power law component for probably intrinsic AGN continuum emissions. The SSP method determined best descriptions to the SDSS spectrum with emission lines being masked out are shown in top panel of Fig. 2 with $\chi^2/dof \sim 1.09$, through the well applied Levenberg-Marquardt least-squares minimization technique. And the corresponding line spectrum is shown in bottom region of panel a in Fig. 2.

Meanwhile, similar fitting procedure was applied to describe the SDSS spectrum with emission lines being masked out in SDSS J2334, only considering the 39 simple stellar population templates but not considering continuum emission component, leading the determined descriptions shown in bottom panel of Fig. 2 with corresponding $\chi^2/dof \sim 1.36$, through the Levenberg-Marquardt least-squares minimization technique. The known F-test technique is applied to confirm confidence level higher than 10σ to support the existence of the power law continuum emission component, after comparing with from different model functions with 2 as the difference between the different $dofs$.

Based on the best descriptions to stellar absorption features, stellar velocity dispersion σ_* is well measured as 112±14km/s, leading the central BH mass to be estimated about $10.2^{+7.6}_{-4.5} \times 10^6 M_\odot$ as shown in Fig. 3 through the well-known $M_{BH} - \sigma_*$ relation (between BH mass and stellar velocity dispersion) (L. Ferrarese & D. Merritt 2000; K. Gebhardt et al. 2000; N. J. McConnell & C.-P. Ma 2013; J. Kormendy & L. C. Ho 2013; M. Batiste et al. 2017; V. N. Bennert et al. 2021) widely accepted in quiescent galaxies (G. A. D. Savorgnan & A. W. Graham 2015), in active galaxies (J.-H. Woo et al. 2015) and also in TDEs (Z. Q. Zhou et al. 2021). The $M_{BH} - \sigma_*$ relation determined BH mass is well consistent with theoretical TDE model determined BH mass, providing further clues to support the central TDE and also support the SSP determined best descriptions in SDSS J2334. Here, in Fig. 3, the 89 quiescent galaxies from G. A. D. Savorgnan & A. W. Graham (2015) and the 29 reverberation mapped AGN from J.-H. Woo et al. (2015) and the 12 TDEs from Z. Q. Zhou et al. (2021) are considered to draw the linear correlation between stellar velocity dispersion and BH mass through the Least Trimmed Squares robust technique (M. Cappellari et al. 2013)

$$\log(\frac{M_{\rm BH}}{10^6 M_\odot}) = (2.22 \pm 0.04) + (4.83 \pm 0.22) \times \log(\frac{\sigma_*}{200{\rm km/s}}). \quad (4)$$

And then the 3σ, 5σ and 6σ confidence bands to the linear correlation are determined and shown in the figure through the F-test technique.

Data for galaxies of all morphological types are available to place on the $M_{\rm BH}$–σ_* diagram. However, it is widely accepted that only massive early-type galaxies, particularly those formed predominantly through 'dry' mergers, are expected to follow $M_{\rm BH}$–σ_* relation (e.g. J. E. Greene et al. (2008); A. E. Reines et al. (2013); I. V. Chilingarian et al. (2018); V. F. Baldassare et al. (2020); K. A. Grishin et al. (2025); J. Kormendy & L. C. Ho (2013)). Therefore, further analysis of the photometric image properties of SDSS J2334 is needed. We have measured its surface brightness profile from the r-band image provided by SDSS to estimate the Sérsic index, as shown in the left panel of Figure 3. The galaxy can be well described with the De Vaucouleurs profile (Sérsic index with n=4) indicated by the red line in the bottom left panel of Figure 3. Considering possible AGN components near the central regions of the galaxy,

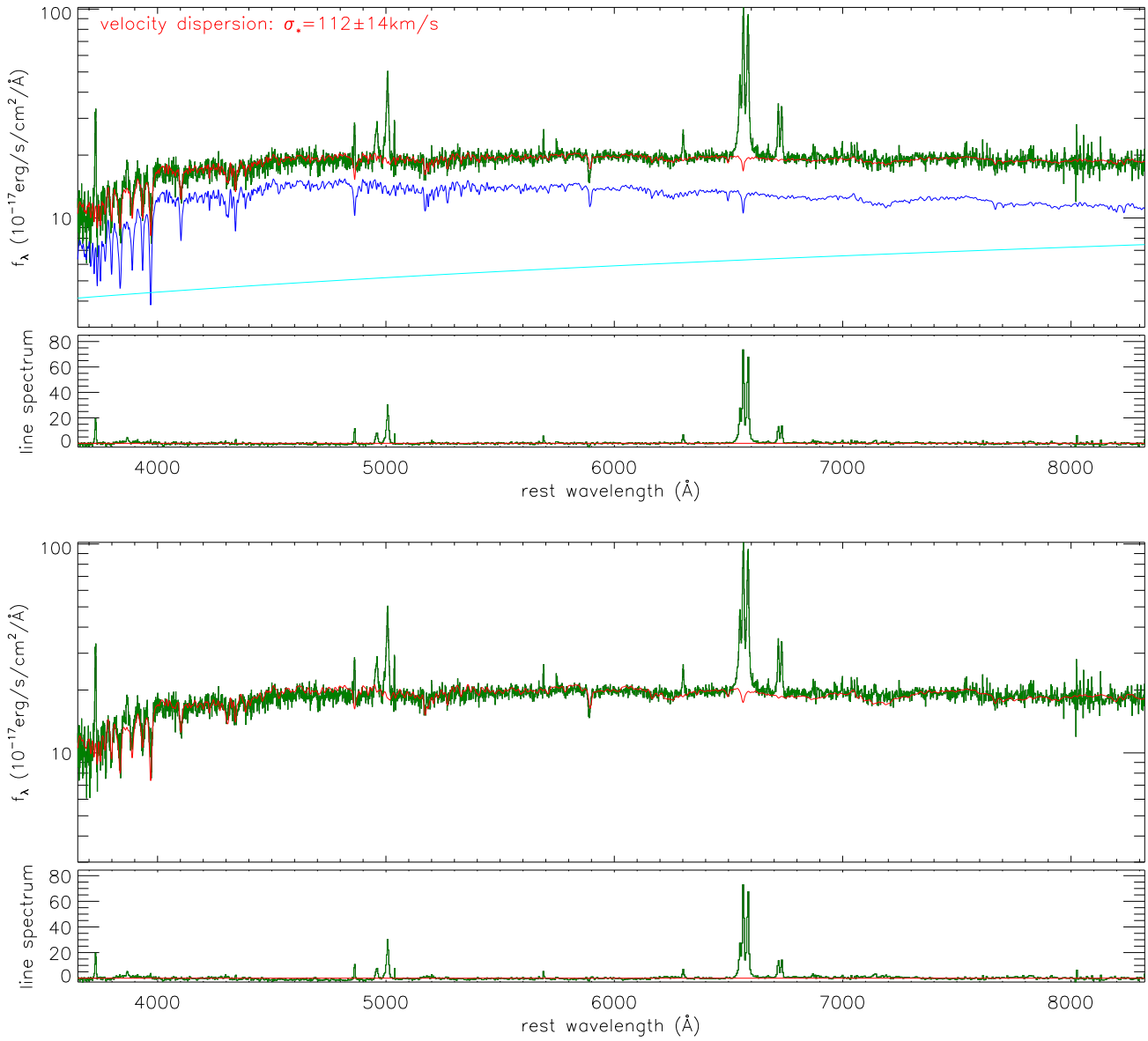

Figure 2. Top panel shows the SDSS spectrum (in dark green) of SDSS J2334 and the SSP method determined best descriptions (in red) including the host galaxy contributions (in blue) and the AGN continuum emissions (in cyan), and the line spectrum in bottom region calculated by SDSS spectrum minus the host galaxy contributions plus the AGN continuum emissions. Bottom panel shows the corresponding results but without considerations of AGN continuum emissions.

the results from 0 to 0.2″of the surface brightness profile are not considered during the fitting procedure. Notably, the elliptical probability of SDSS J2334 provided by the SDSS Galaxy Zoo database (morphological classifications of galaxies (C. Lintott et al. 2011)) is 0.633 with an nvote (the number of votes) of 30, indicating a favorable elliptical galaxy. Therefore, it is acceptable to estimate the black hole mass of SDSS J2334 using the $M_{BH} - \sigma_*$ relation.

After subtracting the host galaxy contributions and AGN continuum emissions (continuum luminosity at rest 5100Å about 7.9×10^{42}erg/s), we can measure the emission lines around the Hβ (from 4800Å to 5050Å) and Hα (from 6480 to 6800Å) in the rest frame including emission lines of Hβ, Hα, [O III]λ4959, 5007Å, [O I]λ6300, 6363Å, and [S II]λ6716, 6731Å doublets, similar as what we have recently done in X. Zhang (2021); X. Zhang & S. Zhao (2022); X.-G. Zhang (2024) and also as done in J. E. Greene & L. C. Ho (2005a); Y. Shen et al. (2011). Due to apparent blue wings in [O III]λ4959, 5007Å doublet in SDSS J2334, there are two Gaussian functions applied to describe

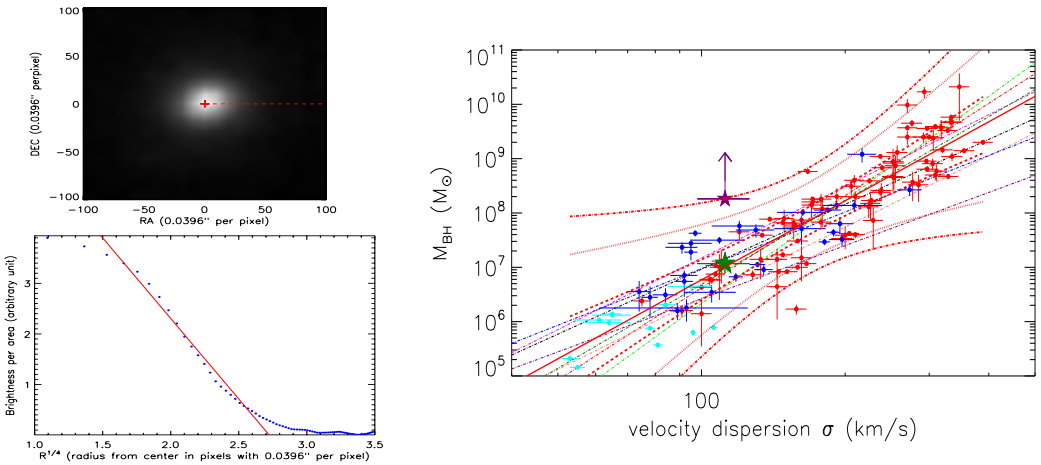

Figure 3. Left panels: the photometric properties of SDSS J2334. The top left panel shows the r-band photometric image cut from the FITS (Flexible Image Transport System) image of the SDSS field, the red cross represents the peak value and the red dashed line represents the positions of obtaining the surface brightness profile. Here, the image is expanded from 10 × 10 pixels to 100 × 100 pixels using the linear interpolation method. The bottom left panel shows the surface brightness profile with horizontal coordinates of $pixel^{1/4}$, and the red solid line indicates the best-fitting results of using a linear function. Right panel: on the correlation between stellar velocity dispersion measured through absorption features and BH mass of SDSS J2334. Solid five-point-star in dark green shows the BH mass of SDSS J2334 determined through applications of theoretical TDE model to long-term light curves. Solid five-point-star in purple shows the virial BH mass determined through assumed broad Balmer emission lines. Dot-dashed lines in green, in red, in magenta, in black, in pink, in purple, in blue and in dark green represent the relations through the quiescent galaxies in G. A. D. Savorgnan & A. W. Graham (2015), in N. J. McConnell & C.-P. Ma (2013), in J. Kormendy & L. C. Ho (2013), and through the RM (reverberation mapped) AGN in J.-H. Woo et al. (2015), the RM AGN with classical bulges in L. C. Ho & M. Kim (2014), the RM AGN with pseudobulges in L. C. Ho & M. Kim (2014) and the RM AGN in J.-H. Woo et al. (2013), and through the TDEs in Z. Q. Zhou et al. (2021), respectively. Solid circles in red, in blue and in pink show the values for the 89 quiescent galaxies from G. A. D. Savorgnan & A. W. Graham (2015), the 29 RM AGN from J.-H. Woo et al. (2015) and the 12 TDEs from Z. Q. Zhou et al. (2021), respectively. Thick solid red line shows the best fitting results to all the objects: the 89 quiescent galaxies, the 29 RM AGN and the 12 TDEs, and thick dashed red lines, thick dotted red lines and thick dot-dashed red lines show the corresponding 3σ, 5σ and 6σ confidence bands to the best fitting results.

the core component and the blue wing of each narrow emission line. The best descriptions to the emission lines and corresponding residuals (calculated by line spectrum minus the best fitting results and then divided by uncertainties of SDSS spectrum) are shown in top panels of Fig. 4 with $\chi^2/dof \sim 0.91$, through the Levenberg-Marquardt least-squares minimization technique. The measured line parameters of each emission line are listed in Table 1. Here, we should note that although extended components for blue wings are applied to describe the [O I] and [S II] doublets, the measured fluxes of the extended components are around zero. Therefore, there are no parameters of extended components of the [O I] and [S II] doublets in Table 1. Considering the determined second moments of the blue-shifted wings in the narrow emission lines, it is not necessary to consider a broad Hα component.

Moreover, besides two Gaussian components applied to describe each component in both [N II] doublet and narrow Hα, three narrow Gaussian components plus a broad Gaussian component were applied to describe emission lines of [N II] doublet and broad Hα and narrow Hα, leading the corresponding best fitting results shown in bottom panels of Fig. 4 with determined $\chi^2/dof \sim 0.97$. In order to confirm the fitting procedure determine broad component in Hα not one broad component from normal central BLRs, the following three points can be clarified. First, considering the Virialization assumptions (M. Vestergaard 2002; B. M. Peterson et al. 2004; J. E. Greene & L. C. Ho 2005b; Y. Shen et al. 2011) to the broad component assumed from central normal BLRs, lower limit of virial BH mass of SDSS J2334 can be estimated as

$$M_{BH} = 5.5\frac{R_{BLRs}\sigma^2_{H\alpha}}{G} \sim 1.8\times10^8 M_\odot \quad (5)$$

with R_{BLRs} estimated by intrinsic continuum luminosity through the R-L empirical relation (M. C. Bentz et al. 2013) and $\sigma_{H\alpha}$ as the second moment of the determined broad Hα, after considering serious obscurations (estimated E(B-V) 2.2 through flux ratio of the determined broad Hα to broad Hβ, relative to the theoretical value 3.1) on broad

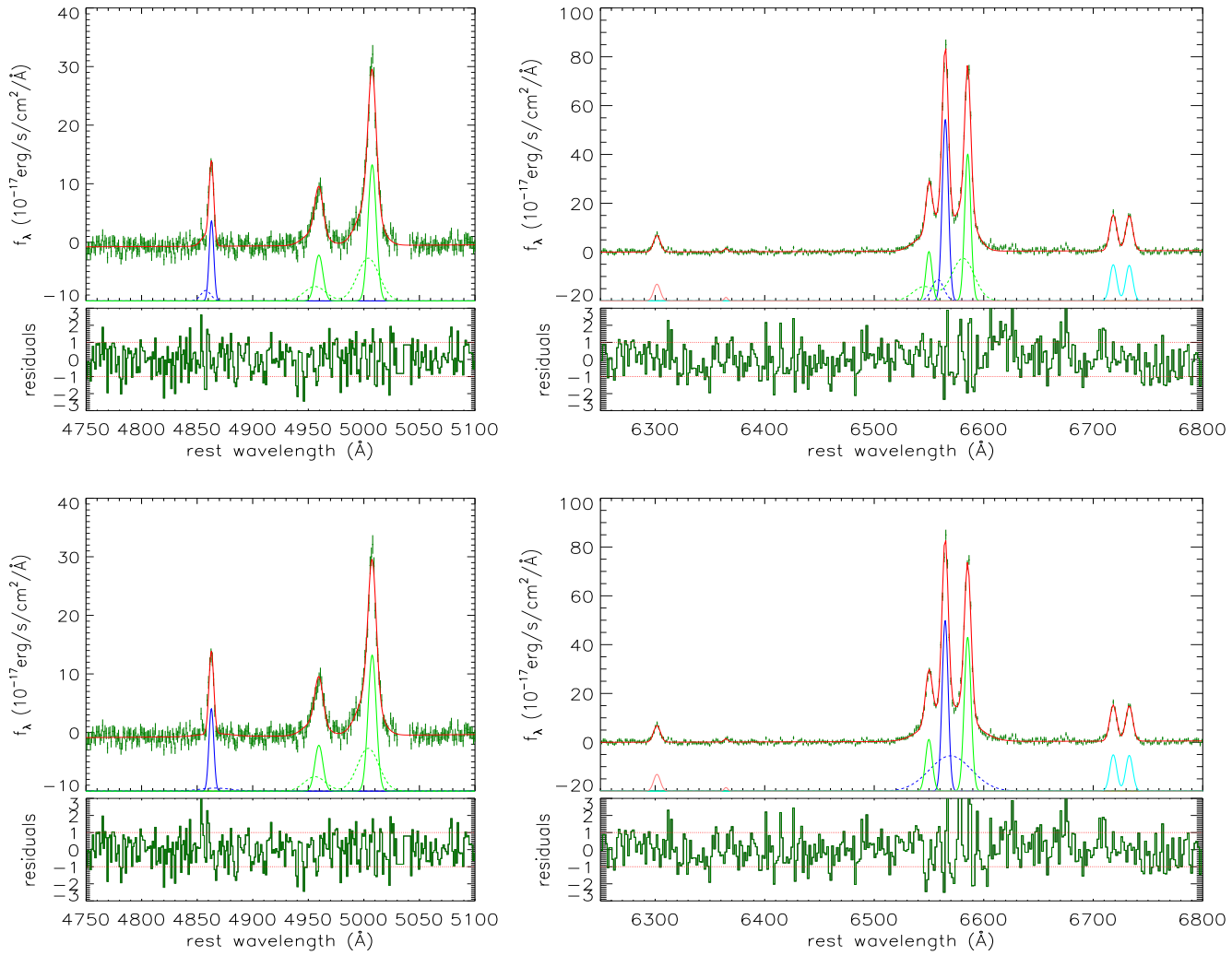

Figure 4. Top panels show the best descriptions (solid line in red) and the corresponding residuals (bottom region) (line spectrum minus the best descriptions and then divided by uncertainties of SDSS spectrum) to the emission lines (small circles plus error bars in dark green) around Hβ and around Hα after considering blue-shifted wings in each narrow emission line. Bottom panels show the best descriptions (solid line in red) and the corresponding residuals (bottom region) to the emission lines (small circles plus error bars in dark green) around Hβ and around Hα after considering broad Balmer emission lines.

Balmer emission lines probably leading to lower line widths of broad emission components. The determined virial BH mass is at least one magnitude higher than the $M_{BH} - \sigma_*$ relation expected BH mass, providing clues to disfavor the determined broad component from normal central BLRs. Second, comparing with the fitting results by different model functions with considering broad Balmer components shown bottom panels of in Fig. 4 and with considering extended components related to radial flows shown in top panels in Fig. 4, the F-test technique can be applied to confirm that the results shown in top panels in Fig. 4 should be preferred with confidence level higher than 6σ (null hypothesis smaller than 10^{-10}). Third, based on the measured continuum luminosity at 5100Å $L_{con} \sim 7.9 \times 10^{42}$erg/s in rest frame without considerations of any obscurations and the linear correlation between L_{con} and the broad Hα line luminosity for normal SDSS quasars as discussed in J. E. Greene & L. C. Ho (2005b), the expected broad Hα line luminosity is about

$$L_{H\alpha_b} = 5.25 \times 10^{42} (\frac{L_{con}}{10^{44}\mathrm{erg/s}})^{1.157}\mathrm{erg/s} \sim 2.7 \times 10^{41}\mathrm{erg/s} \quad (6)$$

which is well consistent with the measured $L_{H\alpha_b} \sim 2.1 \times 10^{41}$erg/s from the assumed broad component in Hα, indicating there were few effects of obscurations providing further clues to support that the determined broad Hα component

Table 1. parameters for the emission lines

line	λ_0	σ	flux
Considering shifted wings in narrow emission lines, with $\chi^2/dof \sim 575.32/631$			
Hβ_n	4862.89±0.06	2.06±0.16	70.8±9.1
Hβ_e	4857.77±2.11	4.40±1.83	19.6±10.9
Hα_n	6564.91±0.09	2.81±0.11	523.6±52.3
Hα_e	6557.98±2.85	5.39±1.68	118.3±55.5
[O III]λ5007Å	5007.48±0.14	3.69±0.19	214.5±20.1
[O III]$_e\lambda$5003Å	5003.98±0.85	9.72±0.79	177.7±20.8
[N II]λ6583Å	6585.39±0.06	2.82±0.07	426.1±15.2
[N II]$_e\lambda$6583Å	6581.01±0.51	10.25±0.48	449.1±15.7
[O I]λ6300Å	6301.61±0.22	3.07±0.25	52.7±3.8
[O I]λ6363Å	6364.63±0.24	1.56±0.79	5.6±2.5
[S II]λ6716Å	6718.29±0.09	3.17±0.08	117.8±4.3
[S II]λ6732Å	6732.91±0.09	3.17±0.09	115.9±4.1
Considering broad component in Balmer emission lines, with $\chi^2/dof \sim 606.38/632$			
Hβ_b	4866.39±0.34	14.18±0.33	18.2±10.8
Hβ_n	4862.80±0.04	2.15±0.14	76.2±4.9
Hα_b	6569.62±0.46	19.15±0.45	692.4±22.7
Hα_n	6564.77±0.05	2.77±0.06	486.6±10.8
[O III]λ5007Å	5007.49±0.14	3.68±0.19	214.2±20.2
[O III]$_e\lambda$5003Å	5003.95±0.85	9.63±0.78	176.1±21.1
[N II]λ6583Å	6585.32±0.05	3.09±0.05	491.1±9.7
[O I]λ6300Å	6301.61±0.22	3.08±0.25	53.1±3.8
[O I]λ6363Å	6364.63±0.24	1.63±0.81	5.9±2.5
[S II]λ6716Å	6718.29±0.09	3.19±0.08	118.9±4.3
[S II]λ6732Å	6732.91±0.09	3.19±0.08	117.1±4.1

Notes: The first column shows which emission component is measured, Hβ_n (Hα_n) means the narrow emission component, Hβ_e (Hα_e) means the blue-shifted wing in Balmer line, Hβ_b (Hα_b) means the broad emission component in Balmer line. [O III]λ5007Å and [O III]$_e\lambda$5007Å mean the core and the extended component in [O III]λ5007Å emission line. [N II]λ5007Å and [N II]$_e\lambda$5007Å mean the core and the extended component in [N II]λ6583Å emission line, when only shifted blue wings considered in each narrow emission line. The second, third and fourth columns show the central wavelength in unit of Å, the second moment in unit of Å and the emission flux in unit of 10^{-17}erg/s/cm^2/Å, of each Gaussian emission component.

should be not the one from common central BLRs. Therefore, based on the discussed three points above, there are no reliable broad emission components from normal central BLRs in SDSS J2334.

Based on the measured line parameters after considering the blue shifted wing in each narrow emission line, the properties of SDSS J2334 are shown in Fig. 5 in the BPT diagrams with emission line ratios calculated through the narrow components of the narrow emission lines. Based on the dividing lines (L. J. Kewley et al. 2001; G. Kauffmann et al. 2003; L. J. Kewley et al. 2006) between AGN and composite galaxies and H II galaxies and LINERs in the BPT diagrams, SDSS J2334 is an AGN, not a LINER (low-ionization nuclear emission-line region) which could have probably different intrinsic physical ionization sources (M. A. Dopita & R. S. Sutherland 1996; R. Cid Fernandes et al. 2011) from BH accreting processes in AGN. Moreover, considering that the spectrum observation of SDSS J2334 occurred

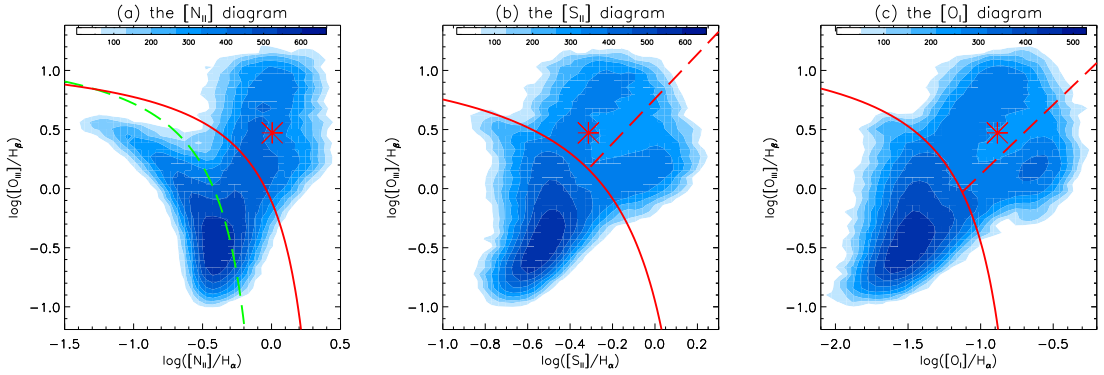

Figure 5. SDSS J2334 (red asterisks) in the BPT diagrams of [O III]/Hβ versus [N II]/Hα (left panel), [O III]/Hβ versus [S II]/Hα (middle panel), and [O III]/Hβ versus [O I]/Hα (right panel), where the contours filled by bluish colors represent properties of all narrow emission line objects collected from SDSS DR16, and solid red lines show the dividing lines between H II galaxies and AGN reported in L. J. Kewley et al. (2001). In the left panel, The dashed green line and solid red line show the dividing lines between H II galaxies and composite galaxies and AGN, reported in G. Kauffmann et al. (2003); L. J. Kewley et al. (2001). In the middle and right panels, dashed red lines show the dividing lines between Seyferts and LINERs reported in L. J. Kewley et al. (2006).

prior to the outburst, there are few effects of TDE emissions on narrow emission lines in spectrum of SDSS J2334. Therefore, based on the spectroscopic properties of SDSS J2334, there are power law continuum emissions, central AGN activities (not related to the central TDE) but no broad emission lines, indicating SDSS J2334 is a candidate of TT2AGN without hidden central BLRs. The emission lines in Figure 4 top panel and the left bottom panel clearly reveal outflow components, which may originate from AGN activity or stellar winds. The primary difference between the two fitting methods is whether the Hα and [N II] fits include outflow components. The analysis of the same SDSS spectrum in the Reference Catalogue of Spectral Energy Distributions version 2 (RCSED2) project [4] (I. V. Chilingarian et al. 2017) suggests that the broad Hα can be explained by an outflow component in Hα and [N II], and this solution is preferred to a broad-line without an outflow component by F-test technique. In addition, RCSED2 also classifies SDSSJ2334 as an AGN based on the BPT diagram. Thus, the results from RCSED2 further support that our results are robust.

Before ending the section, one additional point should be noted. Although the F-test technique and the other methods are applied to accept the existence of the AGN continuum emissions and no apparent broad Balmer emission components included in the SDSS spectrum, the better choice to confirm such spectroscopic features is to do multi-epoch spectroscopic observations in the near future to check whether central AGN variability can lead to expected virialization expected variability of assumed broad Balmer emission components. More candidates like SDSS J2334 identified in the near future should provide further clues to support to to be against the proposed method in the manuscript. At the present stage, through the TDE model determined best descriptions to the photometric variability and the spectroscopic features of no apparent broad Balmer lines, the SDSS J2234 can be accepted as a potential candidate of TT2AGN.

4. DISSCUSSION

4.1. *Mid-infrared/Radio data*

SDSS J2334 has been detected throughout the Wide-field Infrared Survey Explorer (WISE; E. L. Wright et al. (2010)). We have collected archival multiepoch mid-infrared (MIR) photometry from the ALLWISE[5] and the most recent Near-Earth Object WISE (NEOWISE; A. Mainzer et al. (2014)) data releases. The ALLWISE data are only available for two observational epochs (MJD 55368 & MJD 55549). NEOWISE provides a long-term light curve that spans the period from MJD 56645 (Dec. 2013) to MJD 60482 (Jun. 2024), with a half-year cadence. The light curves in W1 and W2 bands are presented in the middle panel of Figure 1. The MIR light curves of SDSS J2334 show a slight rise from WISE, while the data from NEOWISE show a slow decay trend. Due to the large gap between WISE

[4] https://rcsed2.voxastro.org
[5] https://wise2.ipac.caltech.edu/docs/release/allwise/

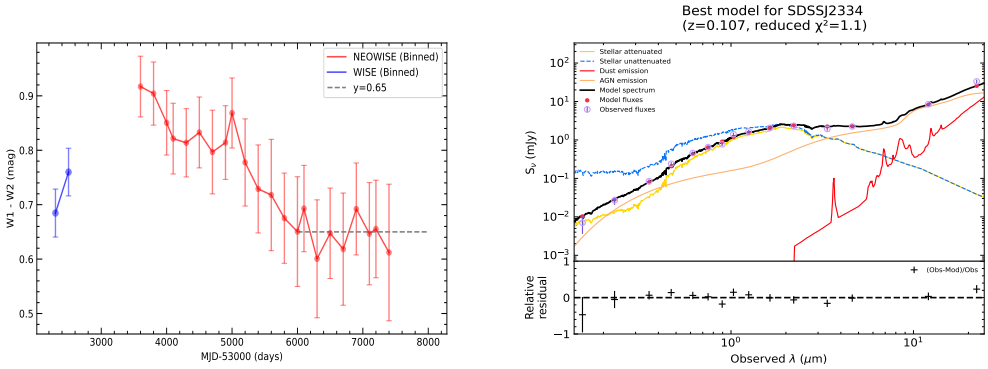

Figure 6. Left panel: W1-W2 evolution of SDSS J2334, with binning applied to the data for each observation period of approximately six months. The gray dashed line represents the average value during the post-flare period. Right panel: SED fitting for SDSS J2334. The black line indicates the best-fitting model. The blue, orange, red, and green lines represent unattenuated stellar, attenuated stellar, dust, and AGN emission, respectively. The lower panel indicates residual of the best fitting.

and NEOWISE, we are unable to conduct a further comparative analysis between the MIR and optical light curves. In the left panel of Figure 3, the variation of WISE color (W1-W2) over time is displayed. The MIR color of SDSS J2334 is observed to turn red during the rise and blue during the decay,[6] possibly due to its optical light curves being characterized by a "rapid rise, short peak, and long tail" (Y. Yao et al. 2025). In addition, the WISE color after the outburst (W1-W2 $\sim$ 0.65) is consistent with the typical value of AGN (R. J. Assef et al. 2018).

We have also collected radio observation data reported by Very Large Array Sky Survey (VLASS; M. Lacy et al. (2020) and Rapid ASKAP Continuum Survey (RACS; D. McConnell et al. (2020)). VLASS observation at 2652 days after the optical peak (MJD=55381) gave 1.176±0.29 mJy at 3 GHz (Y. A. Gordon et al. 2021), while RACS at 3218 days gave 2.069±0.546 mJy at 888 MHz (C. L. Hale et al. 2021). According to these data, the radio spectral index $\alpha = -0.46 \pm 0.28$ (assuming a power-law spectrum $S_\nu \propto \nu^{-\alpha}$) is derived, which is consistent with typical values found in core-dominated AGN (A. Anumarlapudi et al. 2024). Considering that the radio observations were conducted $\sim$ 8 years after the TDE optical peak, we suggest that the radio emission may originate from underlying AGN activity.

4.2. *SED FITTING RESULTS*

To better understand the properties between the host galaxy and AGN in SDSS J2334, we have used the SED fitting code `CIGALE` v0.12.1 (D. Burgarella et al. (2005); S. Noll et al. (2009); M. Boquien et al. (2019)). This code can estimate the physical properties of galaxies and/or AGN. The SED data for SDSS J2334 used in our analysis was obtained from the RCSED2 database. We have performed SED fitting using galaxy-only templates with a χ^2/DOF value of 3.7 and using galaxy + AGN templates with a χ^2/DOF value of 1.1. This shows a better fit quality when including the AGN component. The best fitting results are presented in the right panel of Figure 6. The results reveal a significant AGN contribution to the optical emission, indicating that the central region around the central BH of SDSS J2334 is in the direction of our sight.

4.3. *Alternative explanations for the flare observed in SDSS J2334*

The best descriptions to the optical flares can be accepted evidence to support a central TDE in the SDSS J2334. However, it is necessary to discuss the other explanations to the optical flares in SDSS J2334, such as the additional explanations in M. J. Graham et al. (2017); E. Kankare et al. (2017). Based on the asymmetric profile of the flare in SDSS J2334, the model on microlensing should be disfavoured. After considering the AGN-like spectroscopic features in the following section, the model on supernovae should be disfavored. If accepted the intriguing potential cause of the observed optical flare is a stellar mass binary black hole merger within the dense medium of the central accretion disc, or an AGN flare, the model still provides evidence that the central region around the central BH of the SDSS J2334 is in the direction of our sight, leading to the same clues as provided by the TDE model discussed above. Therefore, based on the TDE model determined best descriptions and the probable explanation by a stellar mass binary black

[6] Due to the large gap between WISE and NEOWISE, the highest flux data point may still be in the rising phase of the light curve.

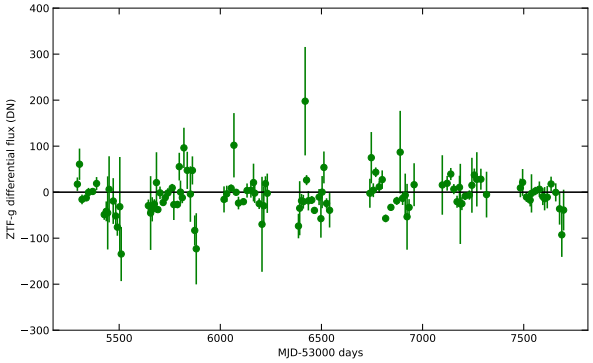

Figure A. Differential fluxes of SDSS J2334 in the ZTF-g filter were binned in groups of 15 consecutive data points, excluding large gaps to keep bins within continuous segments.

hole merger within the central accretion disk (or instability of central accretion disk), we can accept that the central region around central BH of SDSS J2334 is in the direction of our sight.

5. CONCLUSIONS

Candidates for True Type-2 AGN have been previously reported in the literature, not only in low luminosity AGN but also in high luminosity quasars. However, the extreme existence of True Type-2 AGN is still an open question. There are two main reasons leading to mis-classifications of True Type-2 AGN. First, weak optical broad emission lines were overwhelmed in spectroscopic noises. Second, central regions for optical broad emission lines were actually seriously obscured. Here, in SDSS J2334, BH mass properties can be applied to overcome the defect in overwhelmed intrinsic broad emission lines, and the detected TDE can be applied to overcome the defect in seriously obscured central broad line emission regions. In SDSS J2334, TDE properties can be applied to confirm central regions in our line-of-sigh, and meanwhile, spectroscopic properties can be applied to confirm no broad emission lines. Combining the TDE expected variability properties and the spectroscopic features with only narrow emission lines, the SDSS J2234 can be accepted as a potential candidate of True Type-2 AGN. The results provide clues on a new independent technique to identify True Type-2 AGN through unique properties of optical TDEs detected in Type-2 AGN.

ACKNOWLEDGEMENTS

We gratefully acknowledge the anonymous referee for giving us constructive comments and suggestions to greatly improve our paper. We sincerely thank Xin-zhe Wang, Hai-Ming Zhang, You-Dong Hu for useful discussion. This work is supported by the National Natural Science Foundation of China (grants NSFC-12173020, 12373014 and 12133003). Gu gratefully thank the kind financial support from the Innovation Project of Guangxi Graduate Education. The paper has made use of the code of TDEFIT https://tde.space/tdefit/ which is a piece of open-source software written by James Guillochon for the purposes of model-fitting photometric light curves of tidal disruption events and also made use of the code of MOSFIT (Modular Open Source Fitter for Transients) https://mosfit.readthedocs.io/ which is a Python 2.7/3.x package for fitting, sharing, and estimating the parameters of transients via user-contributed transient models. The paper has made use of the MCMC code https://emcee.readthedocs.io/en/stable/index.html.

APPENDIX

A. APPENDIX A:

The forced photometry results of SDSS J2334 are shown in Figure A.

REFERENCES

Ahumada, R., Allende Prieto, C., Almeida, A., et al. 2020, ApJS, 249, 3, doi: 10.3847/1538-4365/ab929e

Antonucci, R. 1993, ARA&A, 31, 473, doi: 10.1146/annurev.aa.31.090193.002353

Antonucci, R. 2012, Astronomical and Astrophysical Transactions, 27, 557, doi: 10.48550/arXiv.1210.2716

Anumarlapudi, A., Dobie, D., Kaplan, D. L., et al. 2024, ApJ, 974, 241, doi: 10.3847/1538-4357/ad64d3

Assef, R. J., Prieto, J. L., Stern, D., et al. 2018, ApJ, 866, 26, doi: 10.3847/1538-4357/aaddf7

Baldassare, V. F., Dickey, C., Geha, M., & Reines, A. E. 2020, ApJL, 898, L3, doi: 10.3847/2041-8213/aba0c1

Barth, A. J., Voevodkin, A., Carson, D. J., & Woźniak, P. 2014, AJ, 147, 12, doi: 10.1088/0004-6256/147/1/12

Batiste, M., Bentz, M. C., Raimundo, S. I., Vestergaard, M., & Onken, C. A. 2017, ApJL, 838, L10, doi: 10.3847/2041-8213/aa6571

Bellm, E. C., Kulkarni, S. R., Graham, M. J., et al. 2019, PASP, 131, 018002, doi: 10.1088/1538-3873/aaecbe

Bennert, V. N., Treu, T., Ding, X., et al. 2021, ApJ, 921, 36, doi: 10.3847/1538-4357/ac151a

Bentz, M. C., Denney, K. D., Grier, C. J., et al. 2013, ApJ, 767, 149, doi: 10.1088/0004-637X/767/2/149

Bianchi, S., Panessa, F., Barcons, X., et al. 2012, MNRAS, 426, 3225, doi: 10.1111/j.1365-2966.2012.21959.x

Bianchi, S., Antonucci, R., Capetti, A., et al. 2019, MNRAS, 488, L1, doi: 10.1093/mnrasl/slz080

Boquien, M., Burgarella, D., Roehlly, Y., et al. 2019, A&A, 622, A103, doi: 10.1051/0004-6361/201834156

Brightman, M., & Nandra, K. 2008, MNRAS, 390, 1241, doi: 10.1111/j.1365-2966.2008.13841.x

Brown, J. S., Holoien, T. W. S., Auchettl, K., et al. 2017, MNRAS, 466, 4904, doi: 10.1093/mnras/stx033

Bruzual, G., & Charlot, S. 2003, MNRAS, 344, 1000, doi: 10.1046/j.1365-8711.2003.06897.x

Bruzual A., G., & Charlot, S. 1993, ApJ, 405, 538, doi: 10.1086/172385

Burgarella, D., Buat, V., & Iglesias-Páramo, J. 2005, MNRAS, 360, 1413, doi: 10.1111/j.1365-2966.2005.09131.x

Burrows, D. N., Kennea, J. A., Ghisellini, G., et al. 2011, Nature, 476, 421, doi: 10.1038/nature10374

Cao, X. 2010, ApJ, 724, 855, doi: 10.1088/0004-637X/724/2/855

Cappellari, M. 2017, MNRAS, 466, 798, doi: 10.1093/mnras/stw3020

Cappellari, M., Scott, N., Alatalo, K., et al. 2013, MNRAS, 432, 1709, doi: 10.1093/mnras/stt562

Chilingarian, I. V., Katkov, I. Y., Zolotukhin, I. Y., et al. 2018, ApJ, 863, 1, doi: 10.3847/1538-4357/aad184

Chilingarian, I. V., Zolotukhin, I. Y., Katkov, I. Y., et al. 2017, ApJS, 228, 14, doi: 10.3847/1538-4365/228/2/14

Cid Fernandes, R., Mateus, A., Sodré, L., Stasińska, G., & Gomes, J. M. 2005, MNRAS, 358, 363, doi: 10.1111/j.1365-2966.2005.08752.x

Cid Fernandes, R., Stasińska, G., Mateus, A., & Vale Asari, N. 2011, MNRAS, 413, 1687, doi: 10.1111/j.1365-2966.2011.18244.x

Dopita, M. A., & Sutherland, R. S. 1996, ApJS, 102, 161, doi: 10.1086/192255

Drake, A. J., Djorgovski, S. G., Graham, M. J., et al. 2019, MNRAS, 482, 98, doi: 10.1093/mnras/sty2673

Drake, A. J., Djorgovski, S. G., Mahabal, A., et al. 2009, ApJ, 696, 870, doi: 10.1088/0004-637X/696/1/870

Elitzur, M. 2012, ApJL, 747, L33, doi: 10.1088/2041-8205/747/2/L33

Elitzur, M., & Ho, L. C. 2009, ApJL, 701, L91, doi: 10.1088/0004-637X/701/2/L91

Elitzur, M., & Netzer, H. 2016, MNRAS, 459, 585, doi: 10.1093/mnras/stw657

Ferrarese, L., & Merritt, D. 2000, ApJL, 539, L9, doi: 10.1086/312838

Foreman-Mackey, D., Hogg, D. W., Lang, D., & Goodman, J. 2013, PASP, 125, 306, doi: 10.1086/670067

Gebhardt, K., Bender, R., Bower, G., et al. 2000, ApJL, 539, L13, doi: 10.1086/312840

Gezari, S. 2021, ARA&A, 59, 21, doi: 10.1146/annurev-astro-111720-030029

Gezari, S., Martin, D. C., Milliard, B., et al. 2006, ApJL, 653, L25, doi: 10.1086/509918

Gezari, S., Chornock, R., Rest, A., et al. 2012, Nature, 485, 217, doi: 10.1038/nature10990

Gordon, Y. A., Boyce, M. M., O'Dea, C. P., et al. 2021, ApJS, 255, 30, doi: 10.3847/1538-4365/ac05c0

Graham, M. J., Djorgovski, S. G., Drake, A. J., et al. 2017, MNRAS, 470, 4112, doi: 10.1093/mnras/stx1456

Greene, J. E., & Ho, L. C. 2005a, ApJ, 627, 721, doi: 10.1086/430590

Greene, J. E., & Ho, L. C. 2005b, ApJ, 630, 122, doi: 10.1086/431897

Greene, J. E., Ho, L. C., & Barth, A. J. 2008, ApJ, 688, 159, doi: 10.1086/592078

Grishin, K. A., Chilingarian, I. V., Combes, F., et al. 2025, arXiv e-prints, arXiv:2502.13202, doi: 10.48550/arXiv.2502.13202

Gu, Y., Zhang, X.-G., Chen, X.-Q., Yang, X., & Liang, E.-W. 2024, MNRAS, doi: 10.1093/mnras/stae2816

Guillochon, J., Manukian, H., & Ramirez-Ruiz, E. 2014, ApJ, 783, 23, doi: 10.1088/0004-637X/783/1/23

Guillochon, J., Nicholl, M., Villar, V. A., et al. 2018, ApJS, 236, 6, doi: 10.3847/1538-4365/aab761

Guillochon, J., & Ramirez-Ruiz, E. 2013, ApJ, 767, 25, doi: 10.1088/0004-637X/767/1/25
Guo, H., Sun, J., Li, S., et al. 2025, ApJ, 979, 235, doi: 10.3847/1538-4357/ada274
Hale, C. L., McConnell, D., Thomson, A. J. M., et al. 2021, PASA, 38, e058, doi: 10.1017/pasa.2021.47
Hammerstein, E., van Velzen, S., Gezari, S., et al. 2023, ApJ, 942, 9, doi: 10.3847/1538-4357/aca283
Hawkins, M. R. S. 2004, A&A, 424, 519, doi: 10.1051/0004-6361:20041127
Ho, L. C., & Kim, M. 2014, ApJ, 789, 17, doi: 10.1088/0004-637X/789/1/17
Ho, L. C., Kim, M., & Terashima, Y. 2012, ApJL, 759, L16, doi: 10.1088/2041-8205/759/1/L16
Huang, X.-X., Wang, J.-X., Tan, Y., Yang, H., & Huang, Y.-F. 2011, ApJL, 734, L16, doi: 10.1088/2041-8205/734/1/L16
Ichikawa, K., Packham, C., Ramos Almeida, C., et al. 2015, ApJ, 803, 57, doi: 10.1088/0004-637X/803/2/57
Kankare, E., Kotak, R., Mattila, S., et al. 2017, Nature Astronomy, 1, 865, doi: 10.1038/s41550-017-0290-2
Kauffmann, G., Heckman, T. M., Tremonti, C., et al. 2003, MNRAS, 346, 1055, doi: 10.1111/j.1365-2966.2003.07154.x
Kewley, L. J., Dopita, M. A., Sutherland, R. S., Heisler, C. A., & Trevena, J. 2001, ApJ, 556, 121, doi: 10.1086/321545
Kewley, L. J., Groves, B., Kauffmann, G., & Heckman, T. 2006, MNRAS, 372, 961, doi: 10.1111/j.1365-2966.2006.10859.x
Kormendy, J., & Ho, L. C. 2013, ARA&A, 51, 511, doi: 10.1146/annurev-astro-082708-101811
Lacy, M., Baum, S. A., Chandler, C. J., et al. 2020, PASP, 132, 035001, doi: 10.1088/1538-3873/ab63eb
Law, N. M., Kulkarni, S. R., Dekany, R. G., et al. 2009, PASP, 121, 1395, doi: 10.1086/648598
Li, Y., Yuan, W., Zhou, H. Y., et al. 2015, AJ, 149, 75, doi: 10.1088/0004-6256/149/2/75
Lintott, C., Schawinski, K., Bamford, S., et al. 2011, MNRAS, 410, 166, doi: 10.1111/j.1365-2966.2010.17432.x
Liu, X.-L., Dou, L.-M., Chen, J.-H., & Shen, R.-F. 2022, ApJ, 925, 67, doi: 10.3847/1538-4357/ac33a9
Mainzer, A., Bauer, J., Cutri, R. M., et al. 2014, ApJ, 792, 30, doi: 10.1088/0004-637X/792/1/30
Masci, F. J., Laher, R. R., Rusholme, B., et al. 2023, arXiv e-prints, arXiv:2305.16279, doi: 10.48550/arXiv.2305.16279
Mattila, S., Pérez-Torres, M., Efstathiou, A., et al. 2018, Science, 361, 482, doi: 10.1126/science.aao4669
McConnell, D., Hale, C. L., Lenc, E., et al. 2020, PASA, 37, e048, doi: 10.1017/pasa.2020.41
McConnell, N. J., & Ma, C.-P. 2013, ApJ, 764, 184, doi: 10.1088/0004-637X/764/2/184
Merloni, A., Dwelly, T., Salvato, M., et al. 2015, MNRAS, 452, 69, doi: 10.1093/mnras/stv1095
Mockler, B., Guillochon, J., & Ramirez-Ruiz, E. 2019, ApJ, 872, 151, doi: 10.3847/1538-4357/ab010f
Nagao, T., Kawabata, K. S., Murayama, T., et al. 2004, AJ, 128, 2066, doi: 10.1086/424936
Netzer, H. 2015, ARA&A, 53, 365, doi: 10.1146/annurev-astro-082214-122302
Noll, S., Burgarella, D., Giovannoli, E., et al. 2009, A&A, 507, 1793, doi: 10.1051/0004-6361/200912497
Peterson, B. M., Ferrarese, L., Gilbert, K. M., et al. 2004, ApJ, 613, 682, doi: 10.1086/423269
Pons, E., & Watson, M. G. 2016, A&A, 594, A72, doi: 10.1051/0004-6361/201629194
Rees, M. J. 1988, Nature, 333, 523, doi: 10.1038/333523a0
Reines, A. E., Greene, J. E., & Geha, M. 2013, ApJ, 775, 116, doi: 10.1088/0004-637X/775/2/116
Savić, D., Goosmann, R., Popović, L. Č., Marin, F., & Afanasiev, V. L. 2018, A&A, 614, A120, doi: 10.1051/0004-6361/201732220
Savorgnan, G. A. D., & Graham, A. W. 2015, MNRAS, 446, 2330, doi: 10.1093/mnras/stu2259
Sazonov, S., Gilfanov, M., Medvedev, P., et al. 2021, MNRAS, 508, 3820, doi: 10.1093/mnras/stab2843
Shen, Y., Richards, G. T., Strauss, M. A., et al. 2011, ApJS, 194, 45, doi: 10.1088/0067-0049/194/2/45
Strubbe, L. E., & Quataert, E. 2009, MNRAS, 400, 2070, doi: 10.1111/j.1365-2966.2009.15599.x
Sun, L., Jiang, N., Dou, L., et al. 2024, A&A, 692, A262, doi: 10.1051/0004-6361/202452380
Tout, C. A., Pols, O. R., Eggleton, P. P., & Han, Z. 1996, MNRAS, 281, 257, doi: 10.1093/mnras/281.1.257
Trakhtenbrot, B., Arcavi, I., MacLeod, C. L., et al. 2019, ApJ, 883, 94, doi: 10.3847/1538-4357/ab39e4
Tran, H. D. 2001, ApJL, 554, L19, doi: 10.1086/320926
Tran, H. D. 2003, ApJ, 583, 632, doi: 10.1086/345473
Urry, C. M., & Padovani, P. 1995, PASP, 107, 803, doi: 10.1086/133630
Valencia-S., M., Zuther, J., Eckart, A., et al. 2012, A&A, 544, A129, doi: 10.1051/0004-6361/201219226
van Velzen, S., Anderson, G. E., Stone, N. C., et al. 2016, Science, 351, 62, doi: 10.1126/science.aad1182
van Velzen, S., Gezari, S., Hammerstein, E., et al. 2021, ApJ, 908, 4, doi: 10.3847/1538-4357/abc258
Veilleux, S., Goodrich, R. W., & Hill, G. J. 1997, ApJ, 477, 631, doi: 10.1086/303735

Vestergaard, M. 2002, ApJ, 571, 733, doi: 10.1086/340045
Wevers, T., Guolo, M., Pasham, D. R., et al. 2024, ApJ, 963, 75, doi: 10.3847/1538-4357/ad1878
Wilhite, B. C., Vanden Berk, D. E., Kron, R. G., et al. 2005, ApJ, 633, 638, doi: 10.1086/430821
Woo, J.-H., Schulze, A., Park, D., et al. 2013, ApJ, 772, 49, doi: 10.1088/0004-637X/772/1/49
Woo, J.-H., Yoon, Y., Park, S., Park, D., & Kim, S. C. 2015, ApJ, 801, 38, doi: 10.1088/0004-637X/801/1/38
Wright, E. L., Eisenhardt, P. R. M., Mainzer, A. K., et al. 2010, AJ, 140, 1868, doi: 10.1088/0004-6256/140/6/1868
Yao, Y., Ye, J., Sun, L., et al. 2025, arXiv e-prints, arXiv:2503.10053, doi: 10.48550/arXiv.2503.10053
Yao, Y., Ravi, V., Gezari, S., et al. 2023, ApJL, 955, L6, doi: 10.3847/2041-8213/acf216
Yip, C. W., Connolly, A. J., Vanden Berk, D. E., et al. 2009, AJ, 137, 5120, doi: 10.1088/0004-6256/137/6/5120
Zakamska, N. L., Schmidt, G. D., Smith, P. S., et al. 2005, AJ, 129, 1212, doi: 10.1086/427543
Zhang, X. 2021, ApJ, 909, 16, doi: 10.3847/1538-4357/abdb35
Zhang, X. 2024, arXiv e-prints, arXiv:2411.12247, doi: 10.48550/arXiv.2411.12247
Zhang, X. 2025, arXiv e-prints, arXiv:2501.16585, doi: 10.48550/arXiv.2501.16585
Zhang, X., YingFei, Z., PeiZhen, C., et al. 2021, ApJ, 922, 248, doi: 10.3847/1538-4357/ac23c8
Zhang, X., & Zhao, S. 2022, ApJ, 937, 105, doi: 10.3847/1538-4357/ac903d
Zhang, X.-G. 2014, MNRAS, 438, 557, doi: 10.1093/mnras/stt2226
Zhang, X.-G. 2022, MNRAS, 516, L66, doi: 10.1093/mnrasl/slac092
Zhang, X.-G. 2024, MNRAS, 534, L23, doi: 10.1093/mnrasl/slae072
Zhou, Z. Q., Liu, F. K., Komossa, S., et al. 2021, ApJ, 907, 77, doi: 10.3847/1538-4357/abcccb